Annu. Rev. Phys. Chem. 2019.70:123-142. Downloaded from www.annualreviews.org
Access provided by 217.212.240.69 on 06/29/20. For personal use only.

ANNUAL REVIEWS

Annual Review of Physical Chemistry

Single Photon Sources in Atomically Thin Materials

Milos Toth and Igor Aharonovich

Institute of Biomedical Materials and Devices, University of Technology Sydney, Ultimo, New South Wales 2007, Australia; email: Milos.Toth@uts.edu.au, Igor.Aharonovich@uts.edu.au

Annu. Rev. Phys. Chem. 2019. 70:123–42

First published as a Review in Advance on February 8, 2019

The *Annual Review of Physical Chemistry* is online at physchem.annualreviews.org

https://doi.org/10.1146/annurev-physchem-042018-052628

Copyright © 2019 by Annual Reviews. All rights reserved

ANNUAL REVIEWS CONNECT

www.annualreviews.org

- Download figures
- Navigate cited references
- Keyword search
- Explore related articles
- Share via email or social media

Keywords

2D materials, nanophotonics, defects, transition metal dichalcogenides, TMDC, hexagonal boron nitride, hBN, quantum information

Abstract

Layered materials are very attractive for studies of light–matter interactions at the nanoscale. In particular, isolated quantum systems such as color centers and quantum dots embedded in these materials are gaining interest due to their potential use in a variety of quantum technologies and nanophotonics. Here, we review the field of nonclassical light emission from van der Waals crystals and atomically thin two-dimensional materials. We focus on transition metal dichalcogenides and hexagonal boron nitride and discuss the fabrication and properties of quantum emitters in these systems and proof-of-concept experiments that provide a foundation for their integration in on-chip nanophotonic circuits. These experiments include tuning of the emission wavelength, electrical excitation, and coupling of the emitters to waveguides, dielectric cavities, and plasmonic resonators. Finally, we discuss current challenges in the field and provide an outlook to further stimulate scientific discussion.

1. INTRODUCTION

The field of layered materials is booming, in part because simple scotch-tape exfoliation often yields high-quality samples with unique photonic and optoelectronic properties (1). Owing to the vast library of van der Waals crystals (2, 3), many laboratories worldwide have shifted their focus to study the optoelectronic properties of atomically thin materials.

The driving force of this field stems from the unique properties of transition metal dichalcogenides (TMDCs) that exhibit a direct bandgap and thus very bright emission when in monolayer form (4). Wafer-scale TMDCs as well as lateral and vertical heterostructures can be grown (5, 6). The TMDCs are used for bright light-emitting diodes (LEDs), low-threshold lasers, advanced photodetectors, and exploration of unique excitonic phenomena (7–9). Among various interesting photophysical properties of the TMDCs (e.g., MoS_2 or WS_2) is the availability of optical readout of the valley state, which is promising for spin physics and valleytronic applications (10–12).

Other emerging materials include transition metal carbides and nitrides that are promising for energy storage and catalysis applications (13). In addition, boron nitride (BN) is often used as a capping protective layer and is thus promising for applications based on polariton and hyperbolic physics (14, 15). Considerable efforts are also dedicated to growing and stabilizing monoatomic layers such as phosphorene (that has a tunable bandgap and thus can be used as a tunable LED) (16–18), germanene (19), or borophene (20). Overall, the exponentially growing library of two-dimensional (2D) materials is enabling the research community to revisit interesting challenges in materials science and physics and to realize new devices.

In addition to these fascinating properties, a compelling aspect of the 2D materials is their applicability to quantum science and technology. Many quantum applications require single photon emitters (SPEs)—isolated quantum systems that emit one photon at a time per excitation cycle that is triggered optically or electrically (21–23). For a detailed overview of the field, we refer the reader to recent reviews (22, 24, 25). Here, we limit the scope to SPEs in layered materials, which can be classified broadly into two types. The first is called a quantum dot (QD). The emission originates from a bound exciton that is confined to zero dimensions by a potential field generated by local strain and/or a crystallographic defect. A QD SPE can be excited directly or by using a higher-energy excitation source that generates a free exciton in the enclosing host material, which is subsequently trapped at the QD. QDs are common in narrow-bandgap materials such as TMDCs, where the bandgap is often smaller than 2.5 eV, and the operation of all presently known SPEs in TMDCs is limited to cryogenic temperatures. The second type of SPE is a color center, an impurity or an isolated crystallographic point defect (a vacancy or an atom at an irregular point in the lattice) with electronic states that lie deep in the bandgap and possess the characteristics of an isolated artificial atom. Color centers are common in wide-bandgap materials such as diamond and silicon carbide, and they are typically excited directly by a sub-bandgap excitation source. Recently, they were also isolated in 2D materials such as hexagonal boron nitride (hBN) (which has a bandgap of approximately 6 eV). Color centers typically act as SPEs not only at cryogenic temperatures but also at and beyond room temperature.

The signature of an SPE is a characteristic dip in the second-order correlation function, $g^2(\tau)$, which correlates arrival times of photons that reach a detector (26). The simplest way to record $g^2(\tau)$ is to split the signal between two avalanche photodiodes and record coincidence counts. A dip below 0.5 at zero delay time, i.e., $g^2(0) < 0.5$, indicates that the emitter is an SPE and that it has an electron density of states characteristic of an isolated zero-dimensional quantum system. Such a measurement can be recorded with either a continuous wave or a pulsed laser. The latter is important for practical applications, such as quantum key distribution, where a triggered source is required. **Figure 1** illustrates the concept of an SPE where a green laser excites a quantum system

Annu. Rev. Phys. Chem. 2019.70:123-142. Downloaded from www.annualreviews.org
Access provided by 217.212.240.69 on 06/29/20. For personal use only.

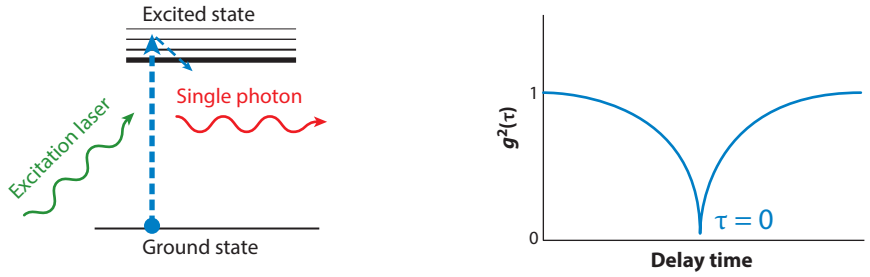

Figure 1

Schematic illustration of a single photon emitter operation. (*a*) An isolated quantum system with a ground and an excited state is pumped using a laser (or electrically) and generates a flux of single photons. (*b*) Schematic illustration of a $g^2(\tau)$ function, with a dip at zero delay time, an indication of a quantum emitter.

(non-resonantly) to a higher vibronic state. After ultrafast nonradiative relaxation to an excited (electronic) state, a photon is emitted as the system relaxes to its ground state. Single photon emission results in non-Poissonian photostatistics, and the $g^2(\tau)$ exhibits a dip at zero delay time. If this dip approaches zero, then the probability of detecting more than one photon at a time is zero, confirming the quantum nature of the detected light.

Over the last decade, many systems have been shown to exhibit single photon emission, including epitaxial and colloidal QDs, single molecules, and carbon dots, as well as defects in various wide-bandgap semiconductors and carbon nanotubes. The emission wavelength varies from the ultraviolet (UV) to the near-infrared (NIR) (~1.5 μm). At present, these systems are increasingly the focus of intense research aimed at achieving brighter and purer sources that can be the basis of scalable quantum nanophotonics platforms. The original pioneering reports of 2D SPE hosts appeared in a set of articles published in 2015 (27–31) and focused on tungsten diselenide (WSe_2), where the SPEs are QDs that operate exclusively at cryogenic temperatures. Shortly after, the first room-temperature SPEs in monolayer and few-layer hosts were discovered in the material hBN (32). These studies initiated the field of quantum emitters in 2D materials. For a general overview of the field of 2D materials, we refer the reader to other recent literature (6, 33).

This review is organized as follows. We first discuss the various available SPEs in these materials, with an emphasis on current understanding of their atomic structure, luminescent properties, and photodynamic properties, before moving on to studies that demonstrate integration of these emitters with dielectric, plasmonic, and photonic devices—the fundamental building blocks of integrated nanophotonic circuits. We conclude with an outlook for the field. **Table 1** summarizes

Table 1 Various two-dimensional material systems that host single photon emitters

Platform	Emission wavelength	Operation temperature	Comments
hBN (32)	Varies, UV-NIR	Room temperature	Brightest of the sources
WO_3 (34)	~620–730 nm	Room temperature	Multilayers produced by thermal annealing of WS_2
WS_2 (35)	~640 nm	Cryogenic	Single/multiple peaks observed in EL/PL spectra
GaSe (36)	~600 nm	Cryogenic	Only multilayers
$MoSe_2$ (37, 38)	~770 nm	Cryogenic	Photon emission statistics not characterized
WSe_2 (27–31)	~730–750 nm	Cryogenic	Also available via electrical excitation

Abbreviations: EL, electroluminescence; hBN, hexagonal boron nitride; PL, photoluminescence.

Annu. Rev. Phys. Chem. 2019.70:123-142. Downloaded from www.annualreviews.org
Access provided by 217.212.240.69 on 06/29/20. For personal use only.

the 2D materials that host SPEs reported to date. Most research has so far been focused on hBN and WSe_2; however, reports of SPEs in other layered materials are constantly emerging.

2. QUANTUM EMITTERS IN TWO-DIMENSIONAL MATERIALS

2.1. Hexagonal Boron Nitride

Most research done to date has been focused on hBN because room-temperature SPE operation has enabled rapid progress with experimental work. hBN resembles diamond in that it has a wide indirect bandgap of ~6 eV (39) and hosts a broad range of SPEs with zero phonon line (ZPL, an emission generated by an electronic transition that does not involve phonons) energies spanning the NIR-visible range (~1.6–2.2 eV) and the UV range (~4.1 eV). The UV SPEs are reported in a cathodoluminescence study (40) performed at 150 K using few-layer flakes of hBN, and the atomic structure of the defect was suggested to be substitutional C on a nitrogen site (C_N) based on prior work on ensembles that luminesce in the same spectral range (41, 42). This assignment has recently been challenged based on calculated C_N transition energies (43), though the calculations are limited to an analysis of charge-state transition levels.

Most research on SPEs in hBN is focused on emitters with ZPLs in the NIR and visible spectral ranges (**Figure 2*a*–*c***). These exhibit a range of promising properties, such as exceptional brightness (>10^6 Hz at the detector in the absence of Purcell enhancement or immersion lens collection schemes), linear in-plane polarization, weak electron–phonon coupling indicated by the low intensity of phonon sidebands (PSBs) in photoluminescence spectra, and exceptional chemical, thermal, and photostability (44, 45). The atomic structure of these emitters is, however, debated, and studies of the structure are complicated by substantial variability in ZPL wavelength (**Figure 2*c***) and in photophysical properties of the emitters. The broad range of emission energies, spanning ~1 eV, observed in samples studied to date suggests that a number of distinct defect structures or defect charge states are responsible for the observed SPEs (45, 46). A number of atomic structures have been considered, with an emphasis on defect complexes composed of nitrogen and boron vacancies (V_N and V_B), and nitrogen, carbon, and oxygen impurities. Theoretical studies have considered dozens of defect structures, and a few have been proposed as possible candidates. Notable examples include the defects in V_NN_B (nitrogen vacancy adjacent to a nitrogen located at a boron site in the lattice), V_NC_B (where C_B is a carbon impurity at a boron site), and V_BO_2 (boron vacancy adjacent to two oxygen impurities) (32, 47–50) (**Figure 2*d*,*e***) that exhibit the in-plane C_2V symmetry exemplified by the defect shown in **Figure 2*d***. In one study, V_B^0 and V_B^- defects were suggested to be dark and bright states of blinking emitters in hBN because B monovacancies were found to be abundant in hBN monolayers studied by transmission electron microscopy and superresolution fluorescence microscopy (51). However, all the assignments made to date are speculative, and more work is needed to determine the atomic structures of emitters in hBN. Most experiments (e.g., ion implantation studies and a comparison of high-purity and carbon-rich hBN) done thus far are inconclusive in this regard (52, 53). Defect assignments suggested by theoretical studies have thus far been limited, in part, by a reliance on comparison of calculated transition energies to measured ZPL energies. This is problematic because numerous defects have allowed transitions within the broad window of ZPLs observed in experiments and are complicated by uncertainties in transition energies calculated using different levels of theory (as discussed in Reference 47).

Deterministic fabrication of emitters in predefined locations in a host is important for scalable engineering of nanophotonic devices and circuits. hBN emitters are present in random locations of some as-grown samples. They can be generated by various postgrowth processing techniques that include annealing, irradiation by ions and low-/high- (keV/MeV) energy electrons (52, 54),

Annu. Rev. Phys. Chem. 2019.70:123-142. Downloaded from www.annualreviews.org
Access provided by 217.212.240.69 on 06/29/20. For personal use only.

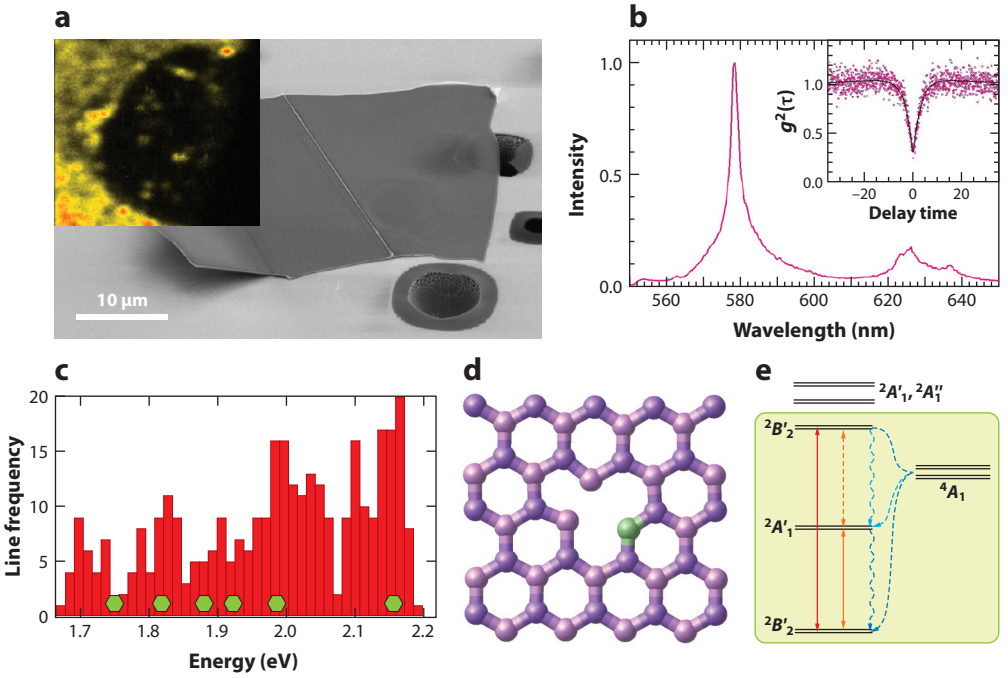

Figure 2

Single photon emitters in hexagonal boron nitride (hBN). (*a*) Scanning electron microscope image of an exfoliated hBN flake. The inset is a confocal map that includes a region of hBN suspended over a hole in the substrate (isolated spots correspond to single emitters). Panel adapted with permission from Reference 58. Copyright 2017, American Chemical Society. (*b*) Typical photoluminescence spectrum of an emitter in hBN consisting of an intense zero phonon line (ZPL) and a phonon side band. The inset is a typical second-order autocorrelation function confirming the quantum nature of the emitter. Panel adapted with permission from Reference 96. Copyright 2018, Royal Society of Chemistry. (*c*) Distribution of ZPL energies in the spectral range of 1.7–2.2 eV. Panel adapted with permission from Reference 46. Copyright 2016, American Chemical Society. (*d*) Schematic illustration of an X_BV_N defect structure where X = N, C, or O. Panel adapted with permission from Reference 48 and the Royal Society of Chemistry. (*e*) Potential electronic level structure of the N_BV_N defect. Panel adapted with permission from Reference 50. Copyright 2018, American Chemical Society.

femtosecond-pulsed laser irradiation (53, 55), plasma processing (49, 56), wet chemical etching (54), and application of a strain field by a periodic array of nanopillars (57). However, in most of these studies, it is unclear whether new defects are produced by the postgrowth processing methods or activated via modification/restructuring of preexisting defects that did not luminesce in the measured spectral range prior to processing. Defect activation seems more likely than creation because all attempts at engineering emitter arrays suffer from low success rate probabilities. Some studies report preferential occurrence of emitters at or near grain boundaries and flake edges, which is undesirable for device applications. However, this is not a universal characteristic, and emitters do also occur well away from edges and extended defects (58).

In addition to emitter locations, it is often also important that the emission energy and dipole orientation are either fixed or engineered deterministically in order to enable fabrication of practical, scalable devices. However, the ZPL energy of emitters in hBN is typically random within a spectral range of ~1.5 to 2.2 eV, although large-area chemical vapor deposition growth of hBN with a much narrower ZPL energy distribution has recently been achieved, as have hBN films grown by molecular beam epitaxy. Some works classify the emitters into two groups characterized by their spectral properties: ZPL energy and shape and PSB intensity (46, 58–62). Most

Annu. Rev. Phys. Chem. 2019.70:123-142. Downloaded from www.annualreviews.org
Access provided by 217.212.240.69 on 06/29/20. For personal use only.

emitters exhibit a PSB doublet that is well separated from the ZPL and located typically ~165 meV below the ZPL. The ZPL width has been observed to scale exponentially with temperature, and this scaling was attributed to piezoelectric coupling to in-plane phonons (46). The emitters are linearly polarized in the plane of hBN, but the dipole orientations do not always correlate with crystallographic axes of hBN (58), and the absorption and emission dipoles can be aligned or misaligned. The latter situation has been shown to correlate with the difference between the ZPL energy and the energy of the excitation laser. It was also attributed to direct excitation into vibronic levels of the first excited electronic state (aligned dipoles) and indirect excitation through an intermediate state (misaligned dipoles) (62). An understanding of these properties will help guide basic studies that aim to elucidate the atomic and electronic structures of the emitters and direct device/application engineering efforts in which the dipole orientation and coupling to the lattice are important.

The excited state lifetime, which governs the ultimate brightness of an (uncoupled) emitter and affects both device performance and signal-to-noise ratios in fundamental studies of these quantum systems, is typically ~3 ns and spans 1 to 10 ns (32, 58, 63, 64). One or more metastable states are typically observed in two-photon correlation measurements (65). Other photophysical properties of the emitters—characterized by dependencies of emission spectra on the wavelength of the excitation laser, blinking and spectral diffusion characteristics, and dipole orientations—vary substantially, likely due in part to variations in local dielectric environment (60, 66–68). While this is problematic for most applications, it is caused primarily by low material quality and is expected to improve as hBN growth techniques are improved in response to the recent surge in interest in the optical properties of hBN. This optimism is justified because some emitters are remarkably stable (69), showing no blinking or bleaching during prolonged photoexcitation, and are able to withstand aggressive environments and processing treatments. For example, robust SPE operation was demonstrated (in vacuum) at temperatures as high as 800 K (70), as was the ability of some SPEs to withstand sequential annealing at 500°C for 1 h each in H_2, O_2, and NH_3 environments. Thus, hBN is appealing for applications such as sensing, which often requires functionality in harsh environments.

However, all emitters in hBN studied to date have been shown to suffer from spectral diffusion (i.e., fluctuations in the wavelength of the emitted photons). This limits minimum line widths obtained in photon coherence time (71) and resonant excitation photoluminescence measurements (64), ultimately limiting quantum applications that require indistinguishable photons. Spectral diffusion is affected primarily by depopulation/population dynamics of charge traps that are adjacent to emitters, and a number of approaches have been used to alter spectra diffusion and blinking/bleaching behavior of emitters in hBN: High and reduced levels of spectral diffusion were observed in hBN flakes on SiO_2 and atomic layer deposition (ALD)–grown Al_2O_3 substrates; blinking of emitters excited by a 708-nm laser was suppressed by coexcitation with a low-power 532-nm laser; and spectral diffusion, blinking, and photobleaching were increased by reducing the excitation wavelength from 532 nm to 405 nm. These phenomena indicate pronounced interactions between emitters and their local environment and the existence of photochemical reactions induced by the excitation laser. Interestingly, one study used He^+ ion bombardment to suppress background luminescence, thus improving the photon purity of an ultrabright quantum emitter (>7 MHz at saturation) from ~0.26 to ~0.08 (61). This was likely due to selective ion-induced modification of defects responsible for background luminescence (a process that is stochastic because He^+ ion bombardment can also destroy emitters and causes sputtering of hBN).

Magneto-optical properties have also been found to vary, suggesting the role of multiple defect species in hBN SPEs. Initial research showed no dependence on applied magnetic fields (59). However, a recent study showed variations in emission intensity and photon emission statistics

Annu. Rev. Phys. Chem. 2019.70:123-142. Downloaded from www.annualreviews.org
Access provided by 217.212.240.69 on 06/29/20. For personal use only.

(bunching caused by metastable states) under magnetic fields at room temperature (72). The field dependencies are highly anisotropic and consistent with a spin-dependent intersystem crossing between triplet and singlet manifolds. This result is significant, as it paves the way to quantum sensing applications and quantum information processing technologies based on optical manipulation and readout of individual spins in hBN.

2.2. Tungsten Diselenide

After hBN, the second most-intensively studied 2D host of quantum emitters is monolayer WSe_2, which has a direct bandgap of ~1.7 eV (27–30). The emitters are NIR QDs attributed to bound excitons that are localized by strain fields. The exciton recombination energy lies ~20–200 meV below that of free 2D excitons; the excited state lifetime and emission line width are on the order of 2 ns and 100 μeV, respectively. Some of the emitters exhibit pronounced Zeeman effects characterized by an extremely high exciton *g*-factor in the range of ~7 to 10 and a zero-field splitting of ~0.7 meV, which indicates that the excitons are confined by an asymmetric potential field. The emission intensity can be modulated (quenched) by an applied electric field. A second class of emitters is characterized by very weak or nonexistent Zeeman splitting (73).

Emitters in WSe_2 typically decorate flake edges and extended defects such as scratches, wrinkles/folds (**Figure 3*a***), and nanobubbles. This is typically attributed to strain fields (74, 75), and strain field anisotropy has been suggested to give rise to linear polarization of emitters. Although initially the emitters were found along the edges of WSe_2 flakes, the subsequent experiments employed strain engineering as a means to generate emitters and tune the emission energy (76, 77). Emitter arrays can be engineered deterministically by a periodic strain field generated by transferring WSe_2 sheets onto nanopillars (**Figure 3*b–d***) (35, 78, 79). The pillar dimensions were not critical to the formation of emitters, and sizes in the range of 100 nm to 300 nm in width/height were tested. The substrate material affects the excited state lifetime, emission line width, blinking, and spectra diffusion characteristics (31, 80). One report suggested that vacancies are involved in the emissions (81), but this is speculative, and more work is needed to confirm this assignment and potential roles of other defects in single photon emission from WSe_2.

2.3. Other Layered Hosts of Single Photon Emitters

Studies on host materials other than hBN and WSe_2 are, to date, limited to a handful on WS_2, $MoSe_2$, GaSe, and WO_3. Electroluminescence measurements of a WS_2 monolayer revealed a quantum emitter characterized by a single peak at ~640 nm, while photoluminescence spectroscopy of the same region yielded multiple peaks in the range of ~610 nm to 660 nm (82). Such emission lines can also be generated deterministically, using a periodic strain field by transferring WS_2 onto an array of dielectric nanopillars. Thermal annealing of WS_2 multilayers at 550°C yields cubic WO_3 that hosts room-temperature quantum emitters in the spectral range of ~620 nm to 730 nm (34). The emitters are linearly polarized and have an excited state lifetime of ~4 ns, but they are not as bright as emitters in hBN, the only other layered host of room-temperature quantum emitters reported so far.

GaSe multilayers contain cryogenic SPEs attributed to bound excitons localized by strain fields attributed to the presence of nanoscale Se inclusions in the multilayers (36). Finally, sharp, spatially localized emission lines at ~770 that have characteristics similar to those of QDs in WSe_2 and WS_2 were also observed in $MoSe_2$ monolayers and multilayers at cryogenic temperatures. The emitters were found in both suspended and supported samples; they also exhibit discrete spectral jumps of a few megaelectron volts induced by an applied voltage and Zeeman splitting characterized by a

Annu. Rev. Phys. Chem. 2019.70:123-142. Downloaded from www.annualreviews.org
Access provided by 217.212.240.69 on 06/29/20. For personal use only.

Annu. Rev. Phys. Chem. 2019.70:123-142. Downloaded from www.annualreviews.org
Access provided by 217.212.240.69 on 06/29/20. For personal use only.

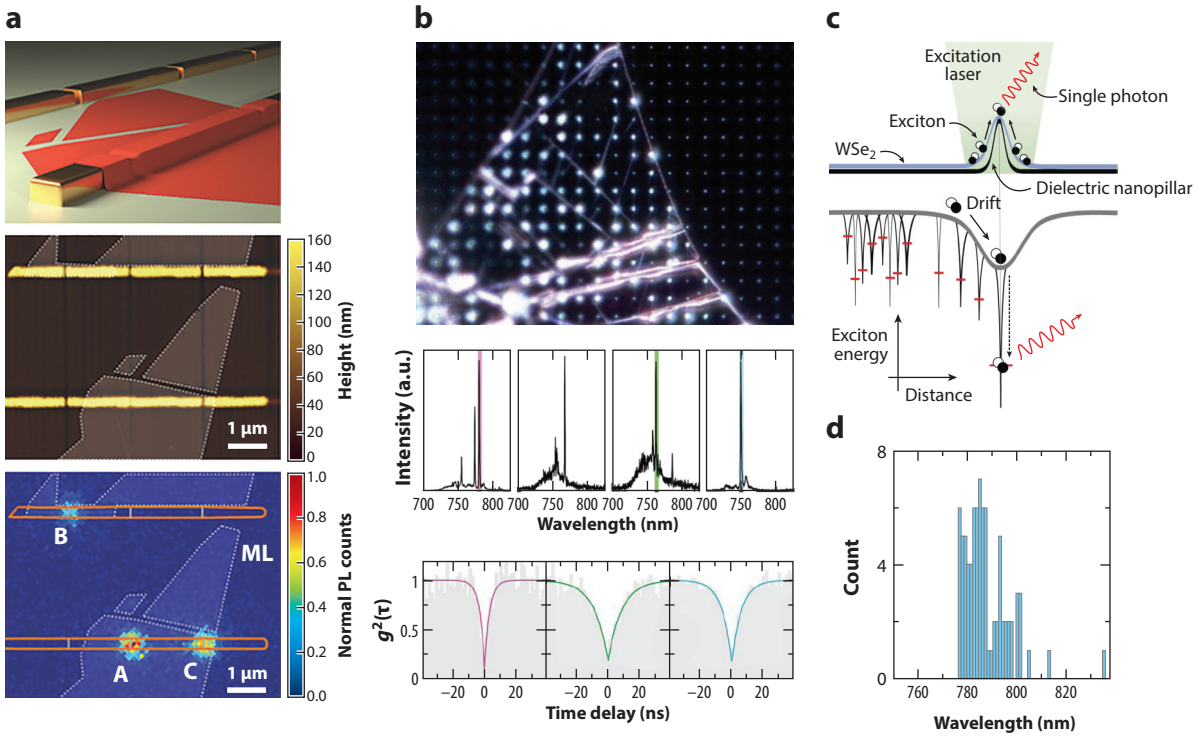

Figure 3

Generation of emitters in WSe_2 by strain field engineering. (*a*) Generation of single emitters localized by a strain field at folds/wrinkles generated by transferring WSe_2 over gaps in gold nanorods. (*Top*) Schematic illustration, (*middle*) optical image, and (*bottom*) a confocal photoluminescence scan showing the formed emitters. Panel adapted with permission from Reference 74. Copyright 2016, John Wiley & Sons. (*b*) Optical image of WSe_2 transferred onto (*top*) an array of SiO_2 nanopillars, (*middle*) representative spectra, and (*bottom*) autocorrelation functions of emitters generated by the pillars. (*c*) Schematic illustration of WSe_2 transferred onto a nanopillar (*top*) and the corresponding potential field that confines the excitons responsible for single photon emission. (*d*) Histogram of the emission wavelength of emitters generated by a pillar array. Panel *b* adapted with permission from Reference 35, panel *c* from Reference 75, and panel *d* from Reference 78 under the terms of the Creative Commons Attribution (CC BY) License, **http://creativecommons.org/licenses/by/4.0**.

g-factor of ∼4 (37, 38). The photon emission statistics of these emitters have, however, not been investigated.

2.4. Electrical Excitation of Single Photon Emitters in Two-Dimensional Materials

Electrical excitation of quantum emitters is important for scalability and on-chip devices. Electrical excitation of defects in 2D TMDCs has been demonstrated using both vertical and horizontal device structures (see **Figure 4**) (82). For the vertical structure, the TMDC (often WSe_2) is placed between thin layers of hBN and graphene layers that act as semitransparent electrodes. A schematic illustration and an optical image of a vertical device are shown in **Figure 4*a***. Fabrication of the device is based on transfer and alignment of multiple 2D layers. Under bias, electrons (holes) tunnel from the negative (positive) electrode to WSe_2 defects. In these experiments, BN acts as a tunnel barrier and enables the formation of excitons within WSe_2 that recombine as both

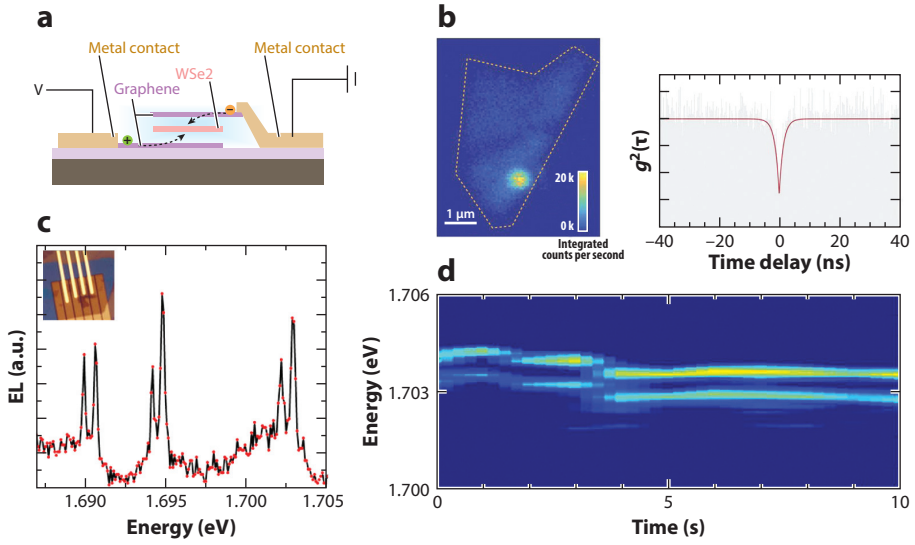

Figure 4

Electrical excitation of single photon emitters (SPEs) in transition metal dichalcogenides (TMDCs). (*a*) Schematic illustration of a vertical device comprised of WSe_2 sandwiched between few-layer boron nitride and metal contacts and an optical image of the device. (*b*) Confocal map and a $g^2(\tau)$ function proving single photon emission. Panel adapted with permission from Reference 82 under the terms of the Creative Commons Attribution (CC BY) License, **http://creativecommons.org/licenses/by/4.0**. (*c*) Electroluminescence (EL) spectrum of numerous SPEs in WSe_2 excited by the horizontal device shown in the inset. (*d*) A corresponding time-dependent photoluminescence trace showing moderate spectral diffusion. Panels *a*, *c*, and *d* adapted with permission from Reference 83. Copyright 2016, American Chemical Society.

free excitons and bound excitons (the latter are localized to defects and give rise to single photon emission). Because the defect-bound excitons are spatially localized, a confocal configuration (often a pinhole in the collection path) is employed for luminescence measurements. A confocal map of such a device and a corresponding antibunching curve that confirms the quantum nature of emission are shown in **Figure 4*b***.

Interestingly, lateral devices with electrostatically defined p-i-n areas also exhibited strong localized emission (**Figure 4*c***) (83). Such flexibility is unique to the 2D nature of the SPE host and is highly advantageous in the design of new quantum optoelectronic devices. **Figure 4*c*** shows an electroluminescence spectrum from a lateral device that contains emission from several isolated defects hosted by WSe_2. Spectral diffusion of these lines is observed over time (**Figure 4*d***). Note that the operation voltages for these devices are rather low, only several volts, which is suitable for scalable on-chip device technologies.

A drawback with devices based on defects in TMDCs is that they operate as SPEs only at cryogenic temperatures. In addition, a broad fluorescence background that overlaps with the quantum emitter lines necessitates the use of efficient narrow band filters to achieve high photon purity.

On the other hand, defects in hBN can be excited at room temperature, though this has not yet been realized using an electrically triggered device due to challenges associated with fabrication of p-n junctions and carrier injection into BN. Although there is no immediate solution to this problem, electrostatic doping techniques could potentially be used as an alternative to conventional quantum LED designs. Other less-optimal techniques may include generation of bandgap

Annu. Rev. Phys. Chem. 2019.70:123-142. Downloaded from www.annualreviews.org
Access provided by 217.212.240.69 on 06/29/20. For personal use only.

UV emission (that can be electrically triggered) that will, in turn, reexcite quantum emitters from the sub-bandgap defects.

2.5. Spectral Tuning of Quantum Emitters

Spectral tuning of quantum emitters is desirable for understanding their properties (e.g., crystallographic structures of defects, defect symmetry, and charge state) and for practical applications such as emission stabilization, coupling to resonators, and generation of indistinguishable photons. Initially, tuning of quantum emitters in hBN was achieved using strain. To apply the strain, hBN flakes hosting the quantum emitters were transferred onto a bendable polycarbonate beam with a high Poisson ratio of 0.37 that results in weak compression perpendicular to the applied tensile strain and vice versa (61). Such modulation resulted in either red or blue shifts of hBN ZPLs, spanning a spectral range of ~6 meV (**Figure 5*a***).

Follow-up experiments showed that tunability under hydrostatic pressure is also possible with a slightly larger tuning range (84) (**Figure 5*b***). Remarkably, hBN withstands high pressures of up to 3 GPa with emitters exhibiting either red or blue shifts. The pressure coefficients varied from approximately −10 meV/GPa to 10 meV/GPa. The authors employed density functional theory (DFT) modeling of the N_BV_N system and concluded that for monolayer hBN, the strain-induced intralayer interaction is dominant, whereas for bilayer flakes, the interlayer interaction component dominates. As a result, emission either red shifts or blue shifts, respectively. For some emitters, a red shift is observed first, followed by a blue shift. This was explained by a corresponding change in the dominant interaction from interlayer to intralayer.

Finally, Stark tuning was also achieved by applying an electric field to single emitters in hBN (**Figure 5*c***) (85). Interestingly, the work was done in a vertical geometry, where the field was applied perpendicular to the flake. This is counterintuitive, as most discussion in the literature is

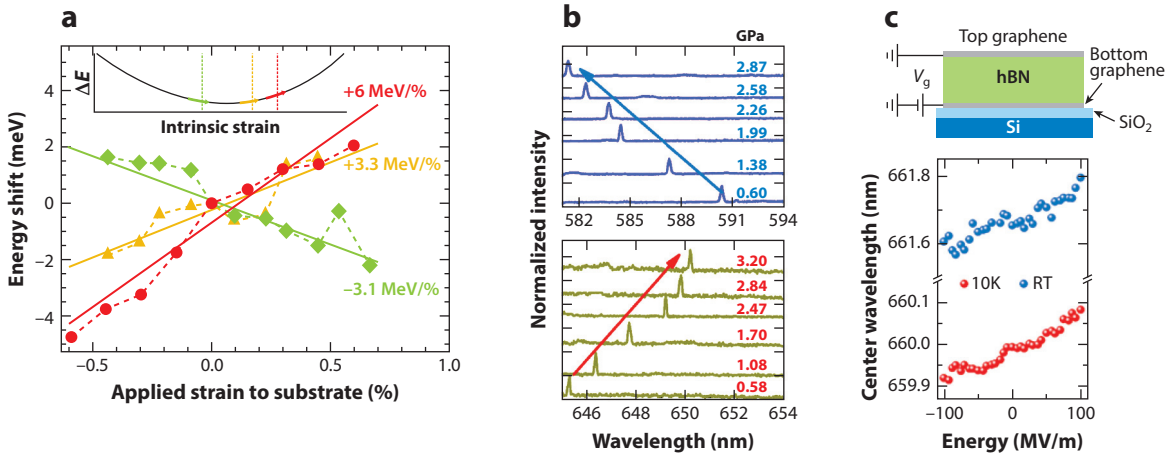

Figure 5

Spectral tuning of quantum emitters in hexagonal boron nitride (hBN). (*a*) Room-temperature (RT) tuning by applied strain. Note that strain can be used to achieve both blue and red shifts of the emission wavelength. Panel adapted with permission from Reference 61 under the terms of the Creative Commons Attribution (CC BY) License, **http://creativecommons.org/licenses/by/4.0**. (*b*) Blue and red shifts induced by the application of hydrostatic pressure to two different emitters that exhibit positive and negative pressure coefficients (performed at cryogenic temperatures). Panel adapted with permission from Reference 84. Copyright 2018, American Chemical Society. (*c*) Bipolar emission tuning by an applied electric field via the Stark effect (performed at both cryogenic temperature and RT). Panel adapted with permission from Reference 85. Copyright 2018, American Chemical Society.

Annu. Rev. Phys. Chem. 2019.70:123-142. Downloaded from www.annualreviews.org
Access provided by 217.212.240.69 on 06/29/20. For personal use only.

Annu. Rev. Phys. Chem. 2019.70:123-142. Downloaded from www.annualreviews.org
Access provided by 217.212.240.69 on 06/29/20. For personal use only.

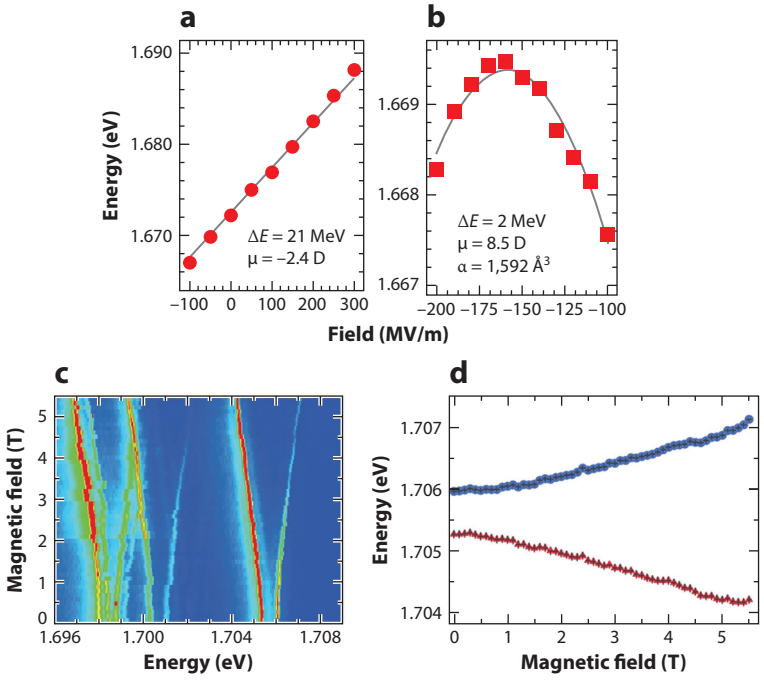

Figure 6

Tuning of single photon emitters in WSe_2 monolayers. (*a*,*b*) Linear and quadratic Stark shift tuning. Panels *a*, *b* adapted with permission from Reference 86. Copyright 2017, American Chemical Society. (*c*,*d*) Zeeman splitting induced by an applied perpendicular magnetic field. Panels *c*, *d* adapted with permission from Reference 29. Copyright Springer Nature.

focused on in-plane defects, yet shifts of up to several nanometers were observed at both room temperature and cryogenic temperatures. Linear, quadratic, and V-shaped Stark shifts were observed. The authors explained the results by modeling the same crystallographic defect of X_BV_N. However, controversially, the atomic impurity is proposed to be located outside of the hBN plane, breaking the planar C_2V symmetry illustrated by **Figure 2*d*** and reducing it to C_1h.

Interestingly, the achieved strain and pressure tuning as well as Stark shift tuning in hBN are larger by almost an order of magnitude than defects in 3D systems such as diamond. Tuning of SPEs in WSe_2 by employing the quantum confined Stark effect was also achieved (86). Both quadratic and linear stark shifts were measured, with shifts of up to ∼21 meV, comparable to semiconductor QDs (see **Figure 6*a*,*b***). Similar to the BN devices, the architecture of the Stark shift is vertical, namely, the WSe_2 monolayers are sandwiched between two BN flakes and two few-layer graphene flakes that act as bottom and top electrodes. Note that only ∼15% of the SPEs in WSe_2 monolayers exhibit a Stark shift.

Zeeman splitting was also realized with similar SPEs in WSe_2 monolayers (27, 29) (**Figure 6*c*,*d***). The magnetic field is applied in a Faraday geometry (perpendicular to the flake). Shifts of tens to hundreds of microelectron volts were achieved with exceptionally high excitonic *g*-factors of up to ∼10. Only ∼60% of the emitters in WSe_2 showed tuning when the magnetic field was applied, while the other emitters remained stable without exhibiting an energy shift. This indicates that the nature and structural origin of the emitters likely vary from location to location and from flake to flake.

3. COUPLING OF SINGLE PHOTON EMITTERS IN TWO-DIMENSIONAL MATERIALS TO PLASMONIC CAVITIES

Plasmonic cavities provide an efficient means to enhance emission from SPEs and can be used to achieve deep-subwavelength confinement volumes. Plasmonic waveguides integrated with SPEs have also been proposed to be used as nanophotonic circuit components (87) but are inherently lossy due to high electron scattering rates. While some proof-of-principle devices have been demonstrated (88, 89), on-chip quantum circuitry has yet to be shown.

The field of plasmonics and 2D materials has been quite active, particularly owing to the properties of graphene (90). In parallel, initial experiments have emerged on coupling of TMDCs to silver cubes and waveguides and resulted in dramatic emission enhancements of more than 20 times (91–94). An important requirement for achieving enhancement is to carefully design a spacer between the 2D TMDC and the plasmonic cavity (i.e., silver cube or gold sphere) so as to avoid fluorescence quenching. This is complicated for quantum emitters in 2D materials due to alignment issues. Therefore, the original work employed periodic plasmonic lattice arrays that are less susceptible to errors in emitter placement accuracy. hBN flakes containing SPEs were precharacterized and transferred onto the lattices (95) (**Figure 7*a***). This enabled a direct comparison of emitters before and after coupling and, hence, an analysis of enhancement of individual quantum systems. Furthermore, the robust, photostable nature of hBN SPEs enabled the emitters to be saturated and therefore to delineate the effects of absorption enhancement and the Purcell effect (i.e., emission enhancement). In an alternative approach, an hBN emitter was precharacterized, and two gold nanoparticles were pushed toward the hBN nanoflake host using an atomic force microscope to achieve coupling (96) (**Figure 7*b***). Such a scheme can potentially be used to realize a horizontal gap cavity. Although this has not been achieved in the initial research on hybrid plasmonic structures based on hBN, a remarkably high count rate exceeding 5×10^6 counts/s was achieved at room temperature with an air objective.

In the field of TMDCs, a silver nanowire was first used as a plasmonic waveguide (**Figure 7*c***) (91). This configuration is interesting because positioning WSe_2 on top of the silver wire yields localized strain fields within WSe_2, and the strain generates SPEs. Top excitation results in propagation of surface plasmon polaritons and light emission from the nanowire, as expected. The overall count rate of this geometry was rather moderate (less than 10^4 counts/s) with ~26% coupling between the emitters and the plasmonic waveguide. Positioning WSe_2 on top of gold pillars has also been demonstrated, but the enhancement was marginal, with overall count rates lower than 10^5 counts/s (94, 97).

A more elegant proposal relied on positioning WSe_2 onto gold pillars and flipping the hybrid structure onto a smooth thin layer of gold (79) (**Figure 7*d***). Such a geometry has two purposes. First, each pillar will generate a localized QD and hence an SPE. Second, the geometry will act as a plasmonic gap cavity. Indeed, in such a scheme a large enhancement of more than a factor of ~10 was achieved, with an impressive count rate. The fluorescence lifetime decreased dramatically, indicating that there is a Purcell enhancement along with a nonradiative recombination pathway. It is important to note that all of these experiments were done at cryogenic temperatures, as QDs in TMDCs are only active at these temperatures. In a way, this defeats one of the main benefits of using plasmonic materials, which is their ability to operate at room temperature. Nonetheless, exploring the advantages of plasmonic gap cavities with SPEs in 2D monolayers is worth pursuing given that the emitters are, by definition, located below the surface of the host material. The next experiments should proceed to coupling to active plasmonic structures that can be dynamically manipulated, exploring chip-scale guiding and realizing ultrabright sources.

Annu. Rev. Phys. Chem. 2019.70:123-142. Downloaded from www.annualreviews.org
Access provided by 217.212.240.69 on 06/29/20. For personal use only.

Annu. Rev. Phys. Chem. 2019.70:123-142. Downloaded from www.annualreviews.org
Access provided by 217.212.240.69 on 06/29/20. For personal use only.

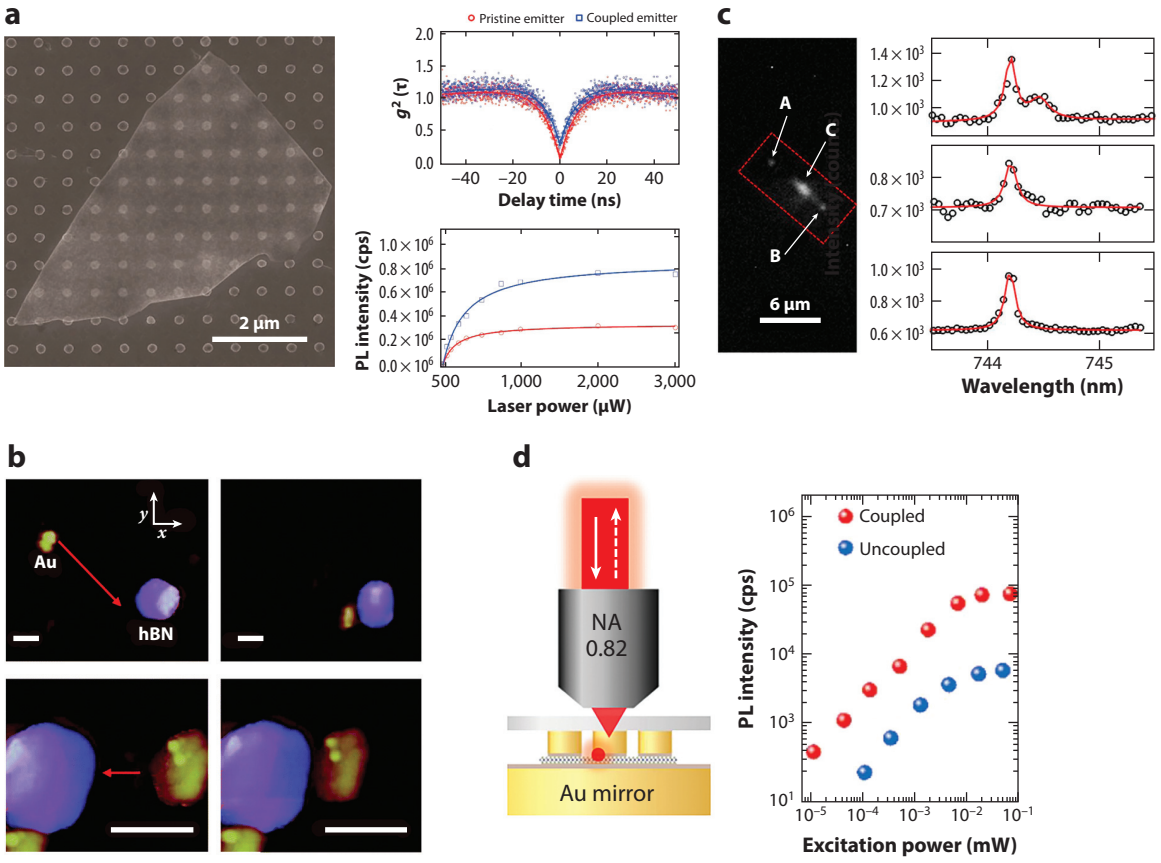

Figure 7

Coupling of single photon emitters (SPEs) in 2D materials to plasmonic nanostructures. (*a*) Few-layer hexagonal boron nitride (hBN) with quantum emitters positioned on top of a plasmonic lattice. Single photon emission is maintained, and a brightness enhancement of ~2 is measured. Panel adapted with permission from Reference 95. Copyright 2017, American Chemical Society. (*b*) Assembly of a hybrid hBN–Au plasmonic cavity by an atomic force microscope. In this geometry, more than 5 million counts/s were measured at room temperature from an SPE. Scale bars = 250 nm. Panel adapted with permission from Reference 96 and the Royal Society of Chemistry. (*c*) WSe_2 is positioned on top of silver that acts as a plasmonic waveguide and naturally activates the emitters. Panel adapted with permission from Reference 91. Copyright 2017, American Chemical Society. (*d*) WSe_2 integrated with a gap cavity where emitters are activated by the pillars. This is one of the brightest emissions from SPEs in WSe_2 reported to date. Panel adapted with permission from Reference 79. Copyright 2018, Springer Nature. Abbreviation: PL, photoluminescence.

4. INTEGRATION OF QUANTUM EMITTERS WITH DIELECTRIC NANOPHOTONIC WAVEGUIDES AND CAVITIES

The integration of 2D materials with nanophotonic cavities has evolved rapidly. This is not surprising given the ease of transfer of 2D flakes and the rather mature nanofabrication techniques of photonic crystals and resonators from silicon nitride or gallium phosphide. Initial results were indeed impressive, with realization of low-threshold lasing from TMDC monolayers positioned on top of a photonic crystal cavity or integrated with a microdisk resonator (7, 98). The advantage of this technique, compared with QD devices, for example, is the elimination of position variation of the dots with regard to the cavity field. Polariton condensates with 2D materials were also demonstrated using a Fabry–Perot type cavity.

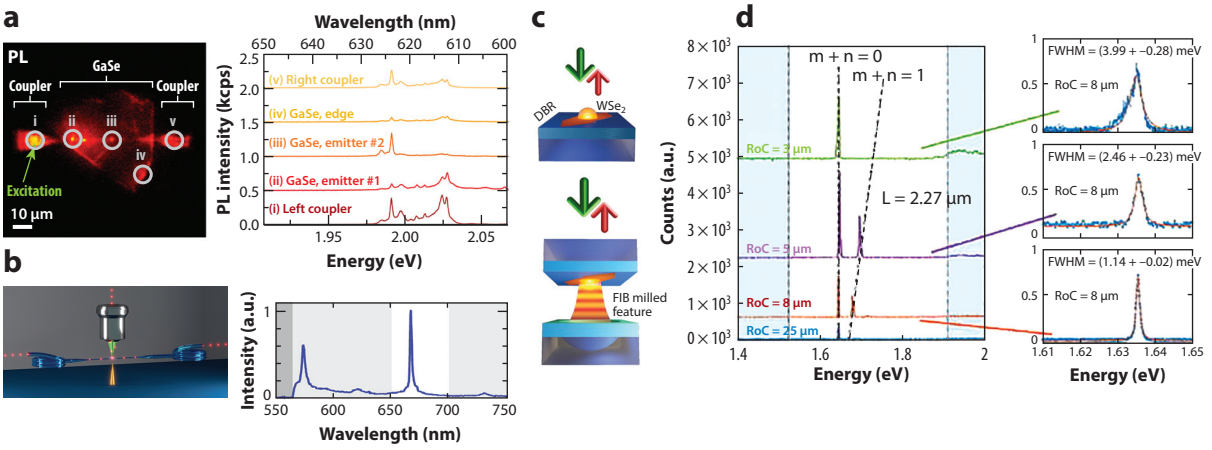

Figure 8

Integration of single photon emitters (SPEs) with waveguides and dielectric cavities. (*a*) Integration of SPEs in GaSe with an on-chip optical waveguide and corresponding spectra recorded with top-down collection and through the waveguide. All measurements were done at cryogenic temperature. Panel adapted with permission from Reference 99. Copyright 2017, American Chemical Society. (*b*) Integration of SPEs in hexagonal boron nitride with an optical waveguide and a room-temperature spectrum recorded through the fiber. Panel adapted with permission from Reference 100. Copyright 2017, American Chemical Society. (*c*) Open Bragg cavity integrated with a quantum emitter in monolayer WSe_2 and (*d*) corresponding spectra of various radii of the milled lens within the Bragg cavity. Panels *c*, *d* adapted with permission from Reference 101. Copyright 2018, AIP Publishing. Abbreviations: DBR, distributed Bragg reflector; FIB, focused ion beam; PL, photoluminescence.

However, the extension of similar methodologies employing quantum emitters in 2D materials is less trivial. This is because the emitters are localized only at particular positions within the flakes, which mandates careful alignment with the photonic device. Consequently, initial results were only achieved with 1D waveguides and optical fibers or waveguides. SPEs in layered GaSe and hBN have been coupled to the waveguides, and the emission was collected using the fiber end or a grating. For the GaSe case (99) (**Figure 8*a***), the work was done at cryogenic temperatures to isolate the narrow QD-like lines. The excitation was performed via the left coupler seen in **Figure 8*a***, and the collection was scanned along the waveguide. It is clearly visible that the excitation light propagates and excites numerous emitters (**Figure 8*a***, lines ii and iii). The quantum nature was maintained, and antibunching curves were recorded from these emitters.

For hBN emitters, the experiments were done at room temperature (100) and on freestanding optical fibers (i.e., not on the substrate) (**Figure 8*b***). The flakes were dispersed randomly onto the optical fiber, and the fluorescence was collected from the top using the same objective (as a reference) or via the fiber edge. Photon statistics were preserved, and the collection efficiency via the fiber end was ∼30%. For these measurements, excitation via the fiber was not possible, but a proper design of the waveguide to improve coupling and filter the propagating laser light is certainly feasible.

The first Purcell enhancement from an emitter in WSe_2 coupled to a microcavity was achieved in an open microcavity (101) (**Figure 8*c*,*d***). A focused ion beam was used to mill concave mirrors into the Bragg cavities to reduce the modal volume. By moving one of the mirrors the cavity mode could be brought into resonance with the SPE. The different mirror sizes resulted in different lineshapes and different cavity quality factors (Q). Under an optimal condition using mirrors with a 5-μm radius, a Purcell enhancement of ∼16 was achieved, associated with enhanced emission and reduced lifetime. The hybrid approach, where an emitter is coupled to a cavity made from a

Annu. Rev. Phys. Chem. 2019.70:123-142. Downloaded from www.annualreviews.org
Access provided by 217.212.240.69 on 06/29/20. For personal use only.

different material, will increasingly be used in experiments over the next few years. Integration of quantum emitters with grating structures and photonic crystals will be of great interest to improve collection efficiencies and realize on-chip devices.

A complementary approach, however, is to focus on the monolithic approach, where the cavity/waveguide is made from the same material. For 2D TMDCs this task is challenging, since the bulk counterparts typically have smaller indirect bandgaps and are absorbing. However, for hBN this is feasible. Preliminary results show that 1D and 2D photonic crystal cavities can be fabricated using advanced lithography and reactive ion etching techniques (102). The cavities have high-quality factors of several thousands in the same spectral range as the quantum emitters. Although questions about cavity tuning and large-scale devices remain open, the process is robust. A further advantage here is the availability of the building block material: multilayered hBN that can simply be exfoliated from a bulk crystal. A similar approach can be extended to other layered materials such as GaSe. The realization of cavities and emitters from the same system is significant, as it introduces real opportunities for integrated quantum photonics with single emitters within van der Waals crystals.

Annu. Rev. Phys. Chem. 2019.70:123-142. Downloaded from www.annualreviews.org
Access provided by 217.212.240.69 on 06/29/20. For personal use only.

5. SUMMARY AND OUTLOOK

SPEs in 2D materials are emerging as promising sources of nonclassical light and will transform the use of 2D materials from classical to quantum technologies. The advanced manipulation techniques of 2D materials and the ability to grow wafer-scale samples will certainly expedite the exploration and controlled engineering of SPEs in these materials. It is interesting, however, that out of the dozens of known 2D compounds currently available, only a few materials were explored in the context of SPEs (see **Table 1**). The search for an ultimate SPE should be extended, with a particular focus on generating SPEs in the telecom band (~1,500 nm). This can potentially be achieved by exploring narrow-bandgap materials such as phosphorene or tellurite compounds. For the known emitters, quantum optical measurements such as two-photon interference need to be demonstrated.

Otherwise, the rapid success in electrical triggering of SPEs in TMDCs should be extended to emitters in wide-bandgap materials such as BN. Although the task is nontrivial, the knowledge gained from the assembly of advanced heterostructures from 2D materials can be utilized, along with new doping techniques available for hBN growth.

Controlled engineering (both spatially and spectrally) of SPEs in these materials also needs further attention. Preliminary results from positioning TMDCs on pillar arrays are a good starting point, but what happens when such TMDCs are removed from the pillars remains unknown (the strain field and hence the emitters are expected to disappear). Localized chemical techniques are perhaps more adequate, similar to those used to stabilize blinking emitters in carbon nanotubes (103). So far, the main disadvantage of the defects in hBN is the lack of optical spin readout, similar to that available for the nitrogen-vacancy center. This is predominantly due to a very different level structure and the group symmetry that lacks an optically accessible triplet state. Initial results on spin-dependent transitions exist, and the study that yielded them should be expanded (72, 104). One plausible way to further tackle this challenge is studying other dopants in hBN, such as transition metals or rare earth elements, that were recently integrated into SiC, YAG, and diamond. Time will show what pathway is the most promising, but identifying single photons with access to the spin degree of freedom is necessary to maintain the momentum.

In terms of applications, super-resolution microscopy has emerged as a promising option for SPEs in hBN. The diversity in photophysical properties was used to realize far-field super-resolution fluorescence imaging of SPEs in hBN using two methods. With the first, blinking was

exploited to temporally resolve emitters separated by ~11 nm. With the second, a resolution of ~63 nm was demonstrated using a new variant of ground-state depletion nanoscopy that exploits a nonlinear photoemission effect exhibited by some emitters in hBN. More studies along these lines are envisioned, particularly as nonlinear excitation (69) and photoluminescence upconversion of single emitters in hBN are becoming possible (105). The recent advances in structuring hBN can pave the way toward interesting optomechanical configurations, as the mechanical properties of BN are already excellent. BN has the additional benefit of possessing quantum emitters (106, 107).

The focused research area of 2D materials inadvertently revived the topic of quantum emitters. Fundamental experiments of emitter-cavity coupling and studies of light–matter interactions with plasmonics resonators have been revisited with these new atomically thin systems. So far, they have showed a better and more powerful performance. The dawn of the quantum flatland is here; however, it has yet to be seen whether the journey is long lived.

DISCLOSURE STATEMENT

The authors are not aware of any affiliations, memberships, funding, or financial holdings that might be perceived as affecting the objectivity of this review.

ACKNOWLEDGMENTS

Financial support from the Australian Research Council (grants DP140102721, DP180100077, LP170100150), the Asian Office of Aerospace Research and Development (grant FA2386-17-1-4064), and the Office of Naval Research Global (grant N62909-18-1-2025) are gratefully acknowledged. I.A. acknowledges the generous support provided by the Alexander von Humboldt Foundation.

LITERATURE CITED

1. Geim AK, Grigorieva IV. 2013. Van der Waals heterostructures. *Nature* 499:419–25
2. Zhou J, Lin J, Huang X, Zhou Y, Chen Y, et al. 2018. A library of atomically thin metal chalcogenides. *Nature* 556:355–59
3. Sahoo PK, Memaran S, Xin Y, Balicas L, Gutiérrez HR. 2018. One-pot growth of two-dimensional lateral heterostructures via sequential edge-epitaxy. *Nature* 553:63–67
4. Mak KF, Shan J. 2016. Photonics and optoelectronics of 2D semiconductor transition metal dichalcogenides. *Nat. Photonics* 10:216–26
5. Lotsch BV. 2015. Vertical 2D heterostructures. *Annu. Rev. Mater. Res.* 45:85–109
6. Novoselov KS, Mishchenko A, Carvalho A, Castro Neto AH. 2016. 2D materials and van der Waals heterostructures. *Science* 353:aac9439
7. Wu S, Buckley S, Schaibley JR, Feng L, Yan J, et al. 2015. Monolayer semiconductor nanocavity lasers with ultralow thresholds. *Nature* 520:69–72
8. Rivera P, Schaibley JR, Jones AM, Ross JS, Wu S, et al. 2015. Observation of long-lived interlayer excitons in monolayer $MoSe_2$–WSe_2 heterostructures. *Nat. Commun.* 6:6242
9. Xu W, Liu W, Schmidt JF, Zhao W, Lu X, et al. 2017. Correlated fluorescence blinking in two-dimensional semiconductor heterostructures. *Nature* 541:62–67
10. Zeng H, Dai J, Yao W, Xiao D, Cui X. 2012. Valley polarization in MoS_2 monolayers by optical pumping. *Nat. Nanotech.* 7:490–93
11. Yang W, Shang J, Wang J, Shen X, Cao B, et al. 2016. Electrically tunable valley-light emitting diode (vLED) based on CVD-grown monolayer WS_2. *Nano Lett.* 16:1560–67

Annu. Rev. Phys. Chem. 2019.70:123-142. Downloaded from www.annualreviews.org
Access provided by 217.212.240.69 on 06/29/20. For personal use only.

12. Hao K, Moody G, Wu F, Dass CK, Xu L, et al. 2016. Direct measurement of exciton valley coherence in monolayer WSe_2. *Nat. Phys.* 12:677–82
13. Naguib M, Mashtalir O, Carle J, Presser V, Lu J, et al. 2012. Two-dimensional transition metal carbides. *ACS Nano* 6:1322–31
14. Caldwell JD, Kretinin AV, Chen Y, Giannini V, Fogler MM, et al. 2014. Sub-diffractional volume-confined polaritons in the natural hyperbolic material hexagonal boron nitride. *Nat. Commun.* 5:5221
15. Dai S, Fei Z, Ma Q, Rodin AS, Wagner M, et al. 2014. Tunable phonon polaritons in atomically thin van der Waals crystals of boron nitride. *Science* 343:1125–29
16. Lu J, Yang J, Carvalho A, Liu H, Lu Y, Sow CH. 2016. Light–matter interactions in phosphorene. *Acc. Chem. Res.* 49:1806–15
17. Walia S, Balendhran S, Ahmed T, Singh M, El-Badawi C, et al. 2017. Ambient protection of few-layer black phosphorus via sequestration of reactive oxygen species. *Adv. Mater.* 29:1700152
18. Yang J, Xu R, Pei J, Myint YW, Wang F, et al. 2015. Optical tuning of exciton and trion emissions in monolayer phosphorene. *Light Sci. Appl.* 4:e312
19. Dávila ME, Xian L, Cahangirov S, Rubio A, Lay GL. 2014. Germanene: a novel two-dimensional germanium allotrope akin to graphene and silicene. *New J. Phys.* 16:095002
20. Mannix AJ, Zhou X-F, Kiraly B, Wood JD, Alducin D, et al. 2015. Synthesis of borophenes: anisotropic, two-dimensional boron polymorphs. *Science* 350:1513–16
21. Wehner S, Elkouss D, Hanson R. 2018. Quantum internet: a vision for the road ahead. *Science* 362:eaam9288
22. Atatüre M, Englund D, Vamivakas N, Lee S-Y, Wrachtrup J. 2018. Material platforms for spin-based photonic quantum technologies. *Nat. Rev. Mater.* 3:38–51
23. Chu X-L, Götzinger S, Sandoghdar V. 2016. A single molecule as a high-fidelity photon gun for producing intensity-squeezed light. *Nat. Photonics* 11:58–62
24. Aharonovich I, Englund D, Toth M. 2016. Solid-state single-photon emitters. *Nat. Photonics* 10:631–41
25. Senellart P, Solomon G, White A. 2017. High-performance semiconductor quantum-dot single-photon sources. *Nat. Nanotechnol.* 12:1026–39
26. Lounis B, Orrit M. 2005. Single-photon sources. *Rep. Prog. Phys.* 68:1129–79
27. Chakraborty C, Kinnischtzke L, Goodfellow KM, Beams R, Vamivakas AN. 2015. Voltage-controlled quantum light from an atomically thin semiconductor. *Nat. Nano* 10:507–11
28. Srivastava A, Sidler M, Allain AV, Lembke DS, Kis A, Imamoğlu A. 2015. Optically active quantum dots in monolayer WSe_2. *Nat. Nanotechnol.* 10:491–96
29. He Y-M, Clark G, Schaibley JR, He Y, Chen MC, et al. 2015. Single quantum emitters in monolayer semiconductors. *Nat. Nanotechnol.* 10:497–502
30. Koperski M, Nogajewski K, Arora A, Cherkez V, Mallet P, et al. 2015. Single photon emitters in exfoliated WSe_2 structures. *Nat. Nanotechnol.* 10:503–6
31. Tonndorf P, Schmidt R, Schneider R, Kern J, Buscema M, et al. 2015. Single-photon emission from localized excitons in an atomically thin semiconductor. *Optica* 2:347–52
32. Tran TT, Bray K, Ford MJ, Toth M, Aharonovich I. 2016. Quantum emission from hexagonal boron nitride monolayers. *Nat. Nanotechnol.* 11:37–41
33. Das S, Robinson JA, Dubey M, Terrones H, Terrones M. 2015. Beyond graphene: progress in novel two-dimensional materials and van der Waals solids. *Annu. Rev. Mater. Res.* 45:1–27
34. Tran TT, Choi S, Scott JA, Xu Z-Q, Zheng C, et al. 2017. Room-temperature single-photon emission from oxidized tungsten disulfide multilayers. *Adv. Opt. Mater.* 5:1600939
35. Palacios-Berraquero C, Kara DM, Montblanch ARP, Barbone M, Latawiec P, et al. 2017. Large-scale quantum-emitter arrays in atomically thin semiconductors. *Nat. Commun.* 8:15093
36. Tonndorf P, Schwarz S, Kern J, Niehues, del Pozo-Zamudio O, et al. 2017. Single-photon emitters in GaSe. *2D Mater.* 4:021010
37. Branny A, Wang G, Kumar S, Robert C, Lassagne B, et al. 2016. Discrete quantum dot like emitters in monolayer $MoSe_2$: spatial mapping, magneto-optics, and charge tuning. *Appl. Phys. Lett.* 108:142101
38. Chakraborty C, Goodfellow KM, Nick Vamivakas A. 2016. Localized emission from defects in $MoSe_2$ layers. *Opt. Mater. Express* 6:2081–87

Annu. Rev. Phys. Chem. 2019.70:123-142. Downloaded from www.annualreviews.org
Access provided by 217.212.240.69 on 06/29/20. For personal use only.

39. Cassabois G, Valvin P, Gil B. 2016. Hexagonal boron nitride is an indirect bandgap semiconductor. *Nat. Photonics* 10:262–66
40. Bourrellier R, Meuret S, Tararan A, Stéphan O, Kociak M, et al. 2016. Bright UV single photon emission at point defects in *h*-BN. *Nano Lett.* 16:4317–21
41. Museur L, Feldbach E, Kanaev A. 2008. Defect-related photoluminescence of hexagonal boron nitride. *Phys. Rev. B* 78:155204
42. Cheng GD, Zhang YG, Yan L, Huang HF, Huang Q, et al. 2017. A paramagnetic neutral C_BV_N center in hexagonal boron nitride monolayer for spin qubit application. *Comput. Mater. Sci.* 129:247–51
43. Weston L, Wickramaratne D, Mackoit M, Alkauskas A, van de Walle CG. 2018. Native point defects and impurities in hexagonal boron nitride. *Phys. Rev. B* 97:214104
44. Martínez LJ, Pelini T, Waselowski V, Maze JR, Gil B, et al. 2016. Efficient single photon emission from a high-purity hexagonal boron nitride crystal. *Phys. Rev. B* 94:121405
45. Tran TT, Elbadawi C, Totonjian D, Gross G, Moon H, et al. 2016. Robust multicolor single photon emission from point defects in hexagonal boron nitride. *ACS Nano* 10:7331–38
46. Jungwirth NR, Calderon B, Ji Y, Spencer MG, Flatt ME, Fuchs GD. 2016. Temperature dependence of wavelength selectable zero-phonon emission from single defects in hexagonal boron nitride. *Nano Lett.* 16:6052–57
47. Reimers JR, Sajid A, Kobayashi R, Ford MJ. 2018. Understanding and calibrating density-functional-theory calculations describing the energy and spectroscopy of defect sites in hexagonal boron nitride. *J. Chem. Theory Comput.* 14:1602–13
48. Tawfik SA, Ali S, Fronzi M, Kianinia M, Tran TT, et al. 2017. First-principles investigation of quantum emission from hBN defects. *Nanoscale* 9:13575–82
49. Xu Z-Q, Elbadawi C, Tran TT, Kianinia M, Li X, et al. 2018. Single photon emission from plasma treated 2D hexagonal boron nitride. *Nanoscale* 10:7957–65
50. Abdi M, Chou J-P, Gali A, Plenio MB. 2018. Color centers in hexagonal boron nitride monolayers: a group theory and ab initio analysis. *ACS Photonics* 5:1967–76
51. Feng J, Deschout H, Caneva S, Hofmann S, Lončarić I, et al. 2018. Imaging of optically active defects with nanometer resolution. *Nano Lett.* 18:1739–44
52. Duong HNM, Nguyen MAP, Kianinia M, Ohshima T, Abe H, et al. 2018. Effects of high-energy electron irradiation on quantum emitters in hexagonal boron nitride. *ACS Appl. Mater. Interfaces* 10:24886–91
53. Choi S, Tran TT, Elbadawi C, Lobo C, Wang X, et al. 2016. Engineering and localization of quantum emitters in large hexagonal boron nitride layers. *ACS Appl. Mater. Interfaces* 8:29642–48
54. Chejanovsky N, Rezai M, Paolucci F, Kim Y, Rendler T, et al. 2016. Structural attributes and photodynamics of visible spectrum quantum emitters in hexagonal boron nitride. *Nano Lett.* 16:7037–45
55. Hou S, Birowosuto MD, Umar S, Anicet MA, Tay RY, et al. 2018. Localized emission from laser-irradiated defects in 2D hexagonal boron nitride. *2D Mater.* 5:015010
56. Vogl T, Campbell G, Buchler BC, Lu Y, Lam PK. 2018. Fabrication and deterministic transfer of high-quality quantum emitters in hexagonal boron nitride. *ACS Photonics* 5:2305–12
57. Proscia NV, Shotan Z, Jayakumar H, Reddy P, Dollar M, et al. 2018. Near-deterministic activation of room temperature quantum emitters in hexagonal boron nitride. *Optica* 5:1128–34
58. Exarhos AL, Hopper DA, Grote RR, Alkauskas A, Bassett LC. 2017. Optical signatures of quantum emitters in suspended hexagonal boron nitride. *ACS Nano* 11:3328–36
59. Li X, Shepard GD, Cupo A, Camporeale N, Shayan K, et al. 2017. Nonmagnetic quantum emitters in boron nitride with ultranarrow and sideband-free emission spectra. *ACS Nano* 11:6652–60
60. Shotan Z, Jayakumar H, Considine CR, Mackoit M, Fedder H, et al. 2016. Photoinduced modification of single-photon emitters in hexagonal boron nitride. *ACS Photonics* 3:2490–96
61. Grosso G, Moon H, Lienhard B, Ali S, Efetov DK, et al. 2017. Tunable and high-purity room temperature single-photon emission from atomic defects in hexagonal boron nitride. *Nat. Commun.* 8:705
62. Jungwirth NR, Fuchs GD. 2017. Optical absorption and emission mechanisms of single defects in hexagonal boron nitride. *Phys. Rev. Lett.* 119:057401
63. Tran TT, Zachreson C, Berhane AM, Bray K, Sandstrom RG, et al. 2016. Quantum emission from defects in single-crystalline hexagonal boron nitride. *Phys. Rev. Appl.* 5:034005

Annu. Rev. Phys. Chem. 2019.70:123-142. Downloaded from www.annualreviews.org
Access provided by 217.212.240.69 on 06/29/20. For personal use only.

64. Tran TT, Kianinia M, Nguyen M, Kim S, Xu Z-Q, et al. 2018. Resonant excitation of quantum emitters in hexagonal boron nitride. *ACS Photonics* 5:295–300
65. Kianinia M, Bradac C, Sontheimer B, Wang F, Tran TT, et al. 2018. All-optical control and super-resolution imaging of quantum emitters in layered materials. *Nat. Commun.* 9:874
66. Schell AW, Svedendahl M, Quidant R. 2018. Quantum emitters in hexagonal boron nitride have spectrally tunable quantum efficiency. *Adv. Mater.* 30:1704237
67. Koperski M, Nogajewski K, Potemski M. 2018. Single photon emitters in boron nitride: more than a supplementary material. *Opt. Commun.* 411:158–65
68. Hernández-Mínguez A, Lähnemann J, Nakhaie S, Lopes JMJ, Santos PV. 2018. Luminescent defects in a few-layer *h*-BN film grown by molecular beam epitaxy. *Phys. Rev. Appl.* 10:044031
69. Schell AW, Tran TT, Takashima H, Takeuchi S, Aharonovich I. 2016. Non-linear excitation of quantum emitters in hexagonal boron nitride multiplayers. *APL Photonics* 1:091302
70. Kianinia M, Regan B, Tawfik SA, Tran TT, Ford MJ, et al. 2017. Robust solid-state quantum system operating at 800 K. *ACS Photonics* 4:768–73
71. Sontheimer B, Braun M, Nikolay N, Sadzak N, Aharonovich I, Benson O. 2017. Photodynamics of quantum emitters in hexagonal boron nitride revealed by low-temperature spectroscopy. *Phys. Rev. B* 96:121202
72. Exarhos AL, Hopper DA, Patel RN, Doherty MW, Bassett LC. 2019. Magnetic-field-dependent quantum emission in hexagonal boron nitride at room temperature. *Nat. Commun.* 10:222
73. Kumar S, Brotóns-Gisbert M, Al-Khuzheyri R, Branny A, Ballesteros-Garcia G, et al. 2016. Resonant laser spectroscopy of localized excitons in monolayer WSe_2. *Optica* 3:882–86
74. Kern J, Niehues I, Tonndorf P, Schmidt R, Wigger D, et al. 2016. Nanoscale positioning of single-photon emitters in atomically thin WSe_2. *Adv. Mater.* 28:7101–5
75. Gabriella DS, Obafunso AA, Xiangzhi L, Zhu XY, James H, Stefan S. 2017. Nanobubble induced formation of quantum emitters in monolayer semiconductors. *2D Mater.* 4:021019
76. Kumar S, Kaczmarczyk A, Gerardot BD. 2015. Strain-induced spatial and spectral isolation of quantum emitters in mono- and bilayer WSe_2. *Nano Lett.* 15:7567–73
77. Ye Y, Dou X, Ding K, Chen Y, Jiang D, et al. 2017. Single photon emission from deep-level defects in monolayer WSe_2. *Phys. Rev. B* 95:245313
78. Branny A, Kumar S, Proux R, Gerardot BD. 2017. Deterministic strain-induced arrays of quantum emitters in a two-dimensional semiconductor. *Nat. Commun.* 8:15053
79. Luo Y, Shepard GD, Ardelean JV, Rhodes DA, Kim B, et al. 2018. Deterministic coupling of site-controlled quantum emitters in monolayer WSe_2 to plasmonic nanocavities. *Nat. Nanotechnol.* 13:1137–42
80. Iff O, He Y-M, Lundt N, Stoll S, Baumann V, et al. 2017. Substrate engineering for high-quality emission of free and localized excitons from atomic monolayers in hybrid architectures. *Optica* 4:669–73
81. Zhang S, Wang C-G, Li M-Y, Huang D, Li L-J, et al. 2017. Defect structure of localized excitons in a WSe_2 monolayer. *Phys. Rev. Lett.* 119:046101
82. Palacios-Berraquero C, Barbone M, Kara DM, Chen X, Goykhman I, et al. 2016. Atomically thin quantum light-emitting diodes. *Nat. Commun.* 7:12978
83. Clark G, Schaibley JR, Ross J, Taniguchi T, Watanabe K, et al. 2016. Single defect light-emitting diode in a van der Waals heterostructure. *Nano Lett.* 16:3944–48
84. Xue Y, Wang H, Tan Q, Zhang J, Yu T, et al. 2018. Anomalous pressure characteristics of defects in hexagonal boron nitride flakes. *ACS Nano* 12:7127–33
85. Noh G, Choi D, Kim J-H, Im D-G, Kim Y-H, et al. 2018. Stark tuning of single-photon emitters in hexagonal boron nitride. *Nano Lett.* 18:4710–15
86. Chakraborty C, Goodfellow KM, Dhara S, Yoshimura A, Meunier V, Vamivakas AN. 2017. Quantum-confined stark effect of individual defects in a van der Waals heterostructure. *Nano Lett.* 17:2253–58
87. Bozhevolnyi SI, Khurgin JB. 2017. The case for quantum plasmonics. *Nat. Photonics* 11:398–400
88. Kewes G, Schoengen M, Neitzke O, Lombardi P, Schönfeld R-S, et al. 2016. A realistic fabrication and design concept for quantum gates based on single emitters integrated in plasmonic-dielectric waveguide structures. *Sci. Rep.* 6:28877

Annu. Rev. Phys. Chem. 2019.70:123-142. Downloaded from www.annualreviews.org
Access provided by 217.212.240.69 on 06/29/20. For personal use only.

89. Hoang TB, Akselrod GM, Mikkelsen MH. 2016. Ultrafast room-temperature single photon emission from quantum dots coupled to plasmonic nanocavities. *Nano Lett*. 16:270–75
90. Iranzo DA, Nanot S, Dias EJC, Epstein I, Peng C, et al. 2018. Probing the ultimate plasmon confinement limits with a van der Waals heterostructure. *Science* 360:291–95
91. Cai T, Dutta S, Aghaeimeibodi S, Yang Z, Nah S, et al. 2017. Coupling emission from single localized defects in two-dimensional semiconductor to surface plasmon polaritons. *Nano Lett*. 17:6564–68
92. Cai T, Kim J-H, Yang Z, Dutta S, Aghaeimeibodi S, Waks E. 2018. Radiative enhancement of single quantum emitters in WSe_2 monolayers using site-controlled metallic nanopillars. *ACS Photonics* 5:3466–71
93. Dutta S, Cai T, Buyukkaya MA, Barik S, Aghaeimeibodi S, Waks E. 2018. Coupling quantum emitters in WSe_2 monolayers to a metal-insulator-metal waveguide. *Appl. Phys. Lett.* 113:191105
94. Tripathi LN, Iff O, Betzold S, Dusanowski Ł, Emmerling M, et al. 2018. spontaneous emission enhancement in strain-induced WSe2 monolayer-based quantum light sources on metallic surfaces. *ACS Photonics* 5:1919–26
95. Tran TT, Wang D, Xu Z-Q, Yang A, Toth M, et al. 2017. Deterministic coupling of quantum emitters in 2D materials to plasmonic nanocavity arrays. *Nano Lett*. 17:2634–39
96. Nguyen M, Kim S, Tran TT, Xu Z-Q, Kianinia M, et al. 2018. Nanoassembly of quantum emitters in hexagonal boron nitride and gold nanospheres. *Nanoscale* 10:2267–74
97. Iff O, Lundt N, Betzold S, Tripathi LN, Emmerling M, et al. 2018. Deterministic coupling of quantum emitters in WSe_2 monolayers to plasmonic nanocavities. *Opt. Express* 26:25944–51
98. Salehzadeh O, Djavid M, Tran NH, Shih I, Mi Z. 2015. Optically pumped two-dimensional MoS_2 lasers operating at room-temperature. *Nano Lett*. 15:5302–6
99. Tonndorf P, Del Pozo-Zamudio O, Gruhler N, Kern J, Schmidt R, et al. 2017. On-chip waveguide coupling of a layered semiconductor single-photon source. *Nano Lett*. 17:5446–51
100. Schell AW, Takashima H, Tran TT, Aharonovich I, Takeuchi S. 2017. Coupling quantum emitters in 2D materials with tapered fibers. *ACS Photonics* 4:761–67
101. Flatten LC, Weng L, Branny A, Johnson S, Dolan PR, et al. 2018. Microcavity enhanced single photon emission from two-dimensional WSe_2. *Appl. Phys. Lett.* 112:191105
102. Kim S, Fröch JE, Christian J, Straw M, Bishop J, et al. 2018. Photonic crystal cavities from hexagonal boron nitride. *Nat. Commun.* 9:2623
103. He X, Htoon H, Doorn SK, Pernice WHP, Pyatkov F, et al. 2018. Carbon nanotubes as emerging quantum-light sources. *Nat. Mater.* 17:663–70
104. Toledo JR, de Jesus DB, Kianinia M, Leal AS, Fantini C, et al. 2018. Electron paramagnetic resonance signature of point defects in neutron-irradiated hexagonal boron nitride. *Phys. Rev. B* 98:155203
105. Wang Q, Zhang Q, Zhao X, Luo X, Wong CPY, et al. 2018. Photoluminescence upconversion by defects in hexagonal boron nitride. *Nano Lett*. 18:6898–905
106. Abdi M, Hwang M-J, Aghtar M, Plenio MB. 2017. Spin-mechanical scheme with color centers in hexagonal boron nitride membranes. *Phys. Rev. Lett.* 119:233602
107. Falin A, Cai Q, Santos EJG, Scullion D, Qian D, et al. 2017. Mechanical properties of atomically thin boron nitride and the role of interlayer interactions. *Nat. Commun.* 8:15815

Annu. Rev. Phys. Chem. 2019.70:123-142. Downloaded from www.annualreviews.org
Access provided by 217.212.240.69 on 06/29/20. For personal use only.

Annual Review of
Physical Chemistry
Volume 70, 2019

Contents

Annu. Rev. Phys. Chem. 2019.70:123-142. Downloaded from www.annualreviews.org
Access provided by 217.212.240.69 on 06/29/20. For personal use only.

Errata

An online log of corrections to *Annual Review of Physical Chemistry* articles may be found at http://www.annualreviews.org/errata/physchem

Annu. Rev. Phys. Chem. 2019.70:123-142. Downloaded from www.annualreviews.org
Access provided by 217.212.240.69 on 06/29/20. For personal use only.